

**DEVELOPMENTS OF NARROW-LINEWIDTH Q-SWITCHED FIBER LASER,
1480 NM RAMAN FIBER LASER, AND FREE SPACE FIBER AMPLIFIERS**

By

Renjie Zhou

A Thesis Submitted to the Faculty of the

COLLEGE OF OPTICAL SCIENCES

In Partial Fulfillment of the Requirements

For the Degree of

MASTER OF SCIENCE

In the Graduate College

THE UNIVERSITY OF ARIZONA

2011

STATEMENT BY AUTHOR

This thesis has been submitted in partial fulfillment of requirements for an advanced degree at the University of Arizona and is deposited in the University Library to be made available to borrowers under rules of the Library.

Brief quotations from this thesis are allowable without special permission, provided that accurate acknowledgment of source is made. Requests for permission for extended quotation from or reproduction of this manuscript in whole or in part may be granted by the author.

SIGNED: _____

Renjie Zhou

APPROVAL BY THESIS DIRECTOR

This thesis has been approved on the date shown below:

Nasser Peyghambarian

Professor of Optical Sciences

Aug 09, 2011 _____

Date

ACKNOWLEDGEMENTS

Firstly, I would like to give my thanks to Profs Wei Shi and Nasser Peyghambarian for their support. In particular, Prof Shi provided me opportunities to do research projects at NP photonics (NPP). During each projects, he taught me useful experiment skills, and making qualitative analysis. Moreover, all of my work at NPP would be impossible without the help from Prof Peyghambarian who has been supporting my study and research throughout my MS study.

Here I also give my thanks to Prof. Khanh Kieu for serving as my thesis committee member and Dr. Arturo Chavez-Pirson who has supported my research at NPP. Special thanks also give to Rick Franco who has been patiently helping me on contract and other administrative issues. At NPP, Carole and Doug have been very useful! Especial thanks to Carole for the delicious Birthday cake she made for me. Also many thanks give to my colleagues at NPP including Elliot, Xiushan, Jie, Nick, Khawlah, Zhidong, etc.

At the College, I give my thanks to Prof. Carl Maes, Gail Varin, Tammy Orr for their help getting my degree. Besides, I want to give my thanks to my friends at the college, including Shenglin Ye, Huimin Leung, Chih-Yu Huang, and etc.

My unique thanks give to Xiaojun Yang for her caring and supporting. Finally, all my achievement should be given to my parents for their continuing support.

Dedicated to my parents

TABLE OF CONTENTS

LIST OF TABLES.....	7
LIST OF ILLUSTRATIONS.....	8
ABSTRACT.....	11
INTRODUCTION	12
CHAPTER I: SEED-INJECTION, Q-SWITCHED, FIBER LASER	14
1.1 Introduction.....	14
1.2 Laser cavity configuration.....	18
1.3 Experimental results	21
1.4 Numerical model.....	27
1.5 Numerical simulation results.....	31
1.6 Conclusion.....	38
CHAPTER II: 1480 NM RAMAN FIBER LASER	39
2.1 Introduction.....	39
2.2 Raman fiber laser theory	40
2.3 Raman fiber laser design.....	42
2.4 Experimental results	43
2.5 Conclusion.....	48
CHAPTER III: FREE SPACE COUPLED FIBER AMPLIFIER	49

3.1 Introduction.....	49
3.2 Pump and signal free-space coupling into the fiber	50
3.3 Experimental results	53
3.4 Nonlinearity study in Thulium fiber using free space coupling technique..	58
3.5 Conclusion.....	60
CHAPTER IV: CONCLUSION AND FUTURE WORK	61
REFERENCES	63

LIST OF TABLES

Table 1-1. Summary of the fiber laser parameters.....	30
Table 3-1. Signal absorption measurement in the Er/Yb fiber.	57
Table 3-2. Signal coupling efficiency to the Er/Yb fiber.	57

LIST OF ILLUSTRATIONS

Fig 1-1. (a) Q-switched Fiber ring cavity configuration. A 1-meter Er-doped fiber is pumped by a 980 nm diode pump laser. The cavity is seeded by a single-frequency fiber laser. A band-pass filter is used to stabilize the operation. The loss of each component is indicated in the figure in unit of dB. (b) The transmission curve of the 1st order of the AOM in one period..... 18

Fig 1-2. Pulse shapes for different AOM rise time at 500 Hz repetition rate. (a) shows a 500 ns single pulse for 1.5 μs rise time; (b) shows a multi-peak pulse for 60 ns rise time. The seed wavelength is 1530 nm..... 21

Fig 1-3. (a) Pulse width versus AOM repetition rate and (b) Pulse shape at 100 kHz repetition rate. The pump, signal, and the AOM transmission shape are fixed (including the rise time, on time, and fall time). 23

Fig 1-4. Output pulse spectrum for two different seed injection wavelengths. (a) correspond to 1530 nm seed injection. Insert, Fabry-Parot scanning spectrum; (b) correspond to 1557 nm seed injection. 24

Fig 1-5. (a) Erbium energy level diagram. The pump is at 980 nm, and the laser transition is at 1530 nm. (b) Simplified laser cavity structure for numerical modeling. The beam propagation in the cavity consists of three parts, i.e., propagation in erbium fiber, propagation in the passive fiber, and transmission

from all the modules in the cavity.	26
Fig 1-6. Pulse characteristics for different AOM rise time. (a) 1.5 μ s rise time; (b) 60 ns rise time.	32
Fig 1-7. Pulse width versus repetition rate.....	34
Fig 1-8. Pulse profile at different repetition rate. (a) 3 kHz; (b) 10 kHz; (c) 50 kHz (d) 100 kHz.	35
Fig 1-9. Population inversion for two different repetition rates. (a) 3 kHz; (b) 30 kHz.	35
Fig 1-10. Pulse profile for different cavity length. The black line represents 2 meters, the blue dash line represents 3 meter cavity, and the red dash line represents 4 meter cavity.....	35
Fig 1-11 Pulse profile for different cavity loss. The green dash line represents 70% transmission, the blue line represents original transmission, and the red dash line represents 130% transmission.	36
Fig 2-1. Cascaded Raman fiber laser cavity for generating output signal at 1480 nm.	42
Fig 2-2. The combined 975 nm 11-diode pump laser output.	43
Fig 2-3. The 1117 nm Yb fiber laser output power vs. pump power at 975 nm. .	44
Fig 2-4. The 1117 nm Yb fiber laser spectrum with two HR gratings	44

Fig 2-5. The 1175 nm Raman fiber laser.	45
Fig 2-6. The 1175, 1240 nm Raman fiber laser	45
Fig 2-7. The 1175, 1240, 1315 nm Raman fiber laser.	46
Fig 2-8. The 1175, 1240, 1315, 1395 nm Raman fiber laser.....	46
Fig 3-1. The experiment set up for the free space fiber amplifier.....	53
Fig 3-2. Output signal power vs. pump current	54
Fig 3-3 Experiment set up for supercontinuum generation in Tellurite fiber..	58
Fig 3-4. The output spectrum at different pump laser repetition rates.	58

ABSTRACT

In the first chapter, a Q-switched fiber laser that is capable of generating transform-limited pulses based on single-frequency fiber laser seeded ring cavity is demonstrated. The output pulse width can be tuned from hundreds of nanoseconds to several microseconds. This Q-switched ring cavity fiber laser can operate over the whole C-band. In addition, a theoretical model is developed to numerically study the pulse characteristics, and the numerical results are in good agreements with the experimental results. In the next chapter, a Raman fiber laser is developed for generating signal at 1480 nm. Initial experimental results has demonstrated generating of Raman laser at 1175 nm, 1240 nm, 1315 nm, and 1395 nm wavelength. Finally, a free space fiber amplifier is studied both theoretically and experimentally. The experimental work has demonstrated signal coupling efficiency up to 90% in the NP highly Er/Yb co-doped phosphate fiber.

INTRODUCTION

This thesis focuses on the development of Q-switched fiber laser, Raman fiber laser, and free space fiber amplifier.

For the first Chapter, a seed-injection, Q-switched, ring-cavity Er-doped fiber laser is introduced. This fiber laser is studied both experimentally and numerically. The experiment results have demonstrated the generation of transform-limited output pulse with pulse-width tunable from hundreds nano-seconds to several micro-seconds. A numerical model is developed to study the output pulse characteristics. Numerical simulation results agree well with the experiments. In addition, the numerical simulation also studied several other cavity parameters that affect the pulse characteristics.

In the second Chapter, a cascaded Raman fiber laser is developed for generating output wavelength at 1480 nm. The theory of Raman laser is first introduced, and then the Raman laser cavity design is proposed. Finally, the experimental results have demonstrated the Raman laser lasing at each shifted wavelength.

A free space fiber amplifier system is studied in Chapter 3. The factors that affect the signal coupling are discussed in detail. Experimental results for signal amplification and fiber absorption measurements are presented. The results have

shown that the signal coupling efficiency can reach up to 90% in the fiber. The signal coupling technique is then applied to study super-continuum generation in a tellurite fiber.

CHAPTER I

SEED-INJECTION, Q-SWITCHED, FIBER LASER

1.1 Introduction

Fiber lasers have compact design and stable operation compared with traditional solid state lasers. In particular, a large variety of monolithic pulsed fiber lasers have been developed in recent years. These fiber laser pulses are suitable for applications in remote sensing [1], LIDAR systems [2], spectroscopic sensing [3-4], laser frequency conversion [5-6], etc. Especially for applications involving spectroscopic sensing and LIDAR, the coherence length and resolution depends on the linewidth and the pulse duration [2], so narrow-linewidth pulses with tunable wavelength and duration are desired.

There are many ways to achieve Q-switching with narrow linewidth and wavelength tuning. The use of a diffraction grating device to achieve wavelength tuning with single-frequency and narrow linewidth has been demonstrated previously [7-8]. Unfortunately, this method needs precise free space alignment and a bulky diffraction grating impacts the cavity size and packaging. Alternatively, a tunable Fiber-Bragg-Grating (FBG) can be integrated into the fiber laser cavity to achieve active Q-switching with narrow linewidth. Cuadrado-Laborde *et al* [9] have demonstrated transform-limited pulses by acoustically perturbing the FBG.

A narrow linewidth pulse is obtained from this laser cavity. However, this method relies on mechanical means to change the FBG transmission spectrum, which needs additional bulky elements, and the tuning speed is limited. Most recently, Williams *et al* [10] demonstrated optical-tuning of a FBG spectrum to achieve high speed Q-switching. However, this method relies on a sophisticated grating inscription technique using femto-second lasers and the loss due to the grating could be high, decreasing the efficiency. The Fiber Bragg Grating approach can achieve narrow linewidth pulses, but the output wavelength cannot be easily tuned within the cavity. Most of the above approaches employed linear cavity configurations. However, a ring cavity configuration can avoid spatial-hole-burning by forcing the wave propagation in either a clockwise or counter-clockwise direction. In this situation, standing waves will not be formed, so single frequency operation is not limited by the linear cavity modes. By limiting the ASE signal in the cavity, a single-frequency (narrow linewidth) pulse can be achieved. Most recently, Popa *et al* [11] demonstrated the use of a graphene saturable absorber with a tunable filter in a ring cavity to limit the ASE spectrum and achieve wavelength tuning, but the linewidth depends heavily on the bandwidth of the filter, which makes it difficult to achieve transform limited pulses. In recently years, Dragic [12-13] demonstrated that by introducing a single frequency seed

into the cavity, the ASE signal can be suppressed, forcing the laser to operate on the frequency of the narrow linewidth seed. Although Q-switched pulses were demonstrated with this approach, the pulse's temporal profile exhibits multi-peak characteristics, which is not desired for many applications.

In this chapter, we demonstrate the use of single-frequency seed injection into an erbium doped, single mode fiber laser ring cavity to achieve transform-limited, pulsed output. By tuning the seed wavelength, the output signal wavelength can also be tuned, without changing the cavity configuration. An output pulse with a smooth, single peaked temporal profile is achieved. The Q-switching is achieved by using an acousto-optic modulator (AOM) in the cavity, which allows fast and controllable switching performance. By controlling the AOM drive signal repetition rate, output pulse widths ranging from hundreds of nanoseconds to several microseconds are achieved. The transform-limited linewidth of the fiber laser pulses was verified by using a fiber-based Fabry-Perot. In order to understand the origin of pulse characteristics, we have developed a numerical model and simulated the pulse formation from the cavity. The AOM transmission and several cavity parameters that can change pulse characteristics are studied. The numerical study is a guide for the fiber laser cavity design, and the numerical results agree well with the experimental results. We believe this is

the first time a numerical model is developed to simulate the pulse formation for this type of laser cavity with comparison to experimental results.

1.2 Laser cavity configuration

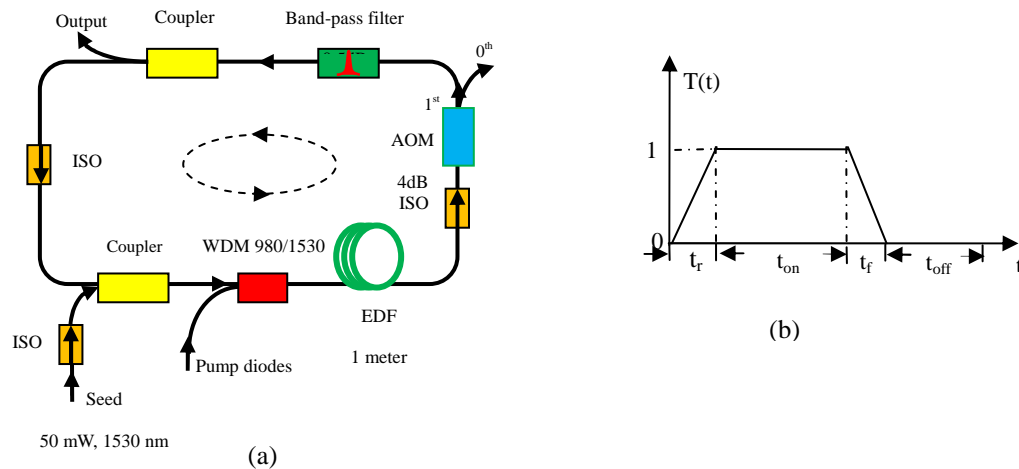


Fig 1-1. (a) Q-switched Fiber ring cavity configuration. A 1-meter Er-doped fiber is pumped by a 980 nm diode pump laser. The cavity is seeded by a single-frequency fiber laser. A band-pass filter is used to stabilize the operation. The loss of each component is indicated in the figure in unit of dB. (b) The transmission curve of the 1st order of the AOM in one period.

The injection seeded ring cavity fiber laser system is depicted in Fig 1-1 (a). The Er-doped fiber is end pumped at 980 nm, and the cavity is seeded by a single-frequency fiber laser at 1530 nm. The laser system is forced to operate in the counter-clockwise direction by using isolators (ISO). Since the beam propagates in one direction, standing wave formation is avoided. Previous experiments demonstrated that by injecting a narrow linewidth seed, the ASE signal can be suppressed, and the laser can operate at the same wavelength as the seed with narrow linewidth [13]. In our experiment, we use a single-frequency fiber laser seed, and the output laser pulses are transform limited centered on the seed

wavelength. The band-pass filter with 100 GHz bandwidth centered at 1530 nm is used to stabilize the cavity operation and suppress ASE, but it does not determine the pulse linewidth.

The Q-switching is achieved by using an AOM, and the AOM transmission is electrically triggered by a function generator. The characteristic of the 1st order transmission of the AOM is shown in Fig 1-1 (b). The AOM transmission curve in one period is divided into four parts: the rise time, on time, the fall time and the off time as shown in Fig. 1-1 (b). The off time determines the repetition rate and the amount of population inversion that is accumulated. When the 1st order transmission of the AOM is switched off (zero transmission), the system is at the low Q cavity mode the Er³⁺ population inversion accumulates. After the AOM transmission is switched on, the cavity Q becomes high and a short pulse is formed. The rise time of the AOM transmission plays an important role in determining the Q-switched pulse profile. Typically, with a very short rise time (~10's of ns) the population inversion will be consumed quickly, resulting in a temporal pulse shape with multiple peaks [14-15]. This phenomenon is also observed in both our experiments and numerical simulations. The AOM open time (including the rise time, on time, and the fall time) is also an important parameter that determines the pulse characteristics. Especially, the maximum

pulse width is limited by the AOM open time. In addition, we demonstrated pulse width tuning by tuning the AOM repetition rate experimentally and numerically. Moreover, in the numerical simulation section, we will discuss how the cavity parameters such as the cavity losses and cavity length can affect the pulse characteristics.

1.3 Experimental results

The experimental set up is described in Fig 1-1(a). A 1-meter single mode (SM), polarization maintaining (PM) Er-doped fiber is used as the gain fiber. The passive fiber used is PM 1550 fiber which has a length of about 1 meter, thus making the total cavity length about 2 meters. The ~ 800 mW pump diodes at 980 nm and a 50-mW fiber laser seed at 1530 nm were used in Fig. 1-1.

1.3.1 AOM rise time

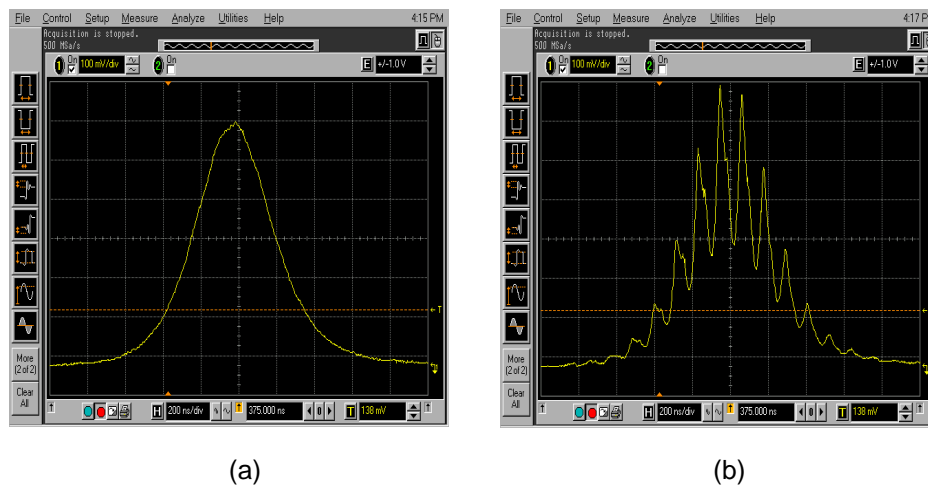


Fig 1-2. Pulse shapes for different AOM rise time at 500 Hz repetition rate. (a) shows a 500 ns single pulse for 1.5 μ s rise time; (b) shows a multi-peak pulse for 60 ns rise time. The seed wavelength is 1530 nm.

We observed that in order to achieve smooth Q-switched pulses, the AOM rise time needs to be longer than a critical value. For example, when the repetition rate is 500 Hz, the AOM rise time should be longer than ~ 300 ns. As shown in

Fig 1-2(a), when the AOM rise time is about $1.5 \mu\text{s}$, a normal Q-switched pulse with 500 ns duration is observed. However, when the AOM rise time is about 60 ns, the pulse exhibits multi-peak characteristics as shown in Fig. 1-2 (b), as reported previously both numerically and experimentally in Ref [14]. The reason for this multi-peak pulse shape is explained as: during the initial time of the pulse formation, the ASE is almost rectangular in time domain; however, as the ASE is amplified through many round-trips in the cavity, the front edge of the ASE is amplified more than the back edge due to the rapid population depletion which is caused by the short rise time. Since the output pulse consists of a sequence of partially extracted ASE signal, the output pulse exhibits multi-peak features. The multi-peak pulse is also obtained through our numerical simulation in Section 5.

1.3.2 Repetition rate

In this section, we fix the pump, signal, and the AOM transmission shape, (i.e., the rise time, on time and fall time are fixed) and then we study the pulse width with regard to the AOM repetition rate. It is found that the pulse width increases with increasing repetition rate - shown in Fig. 1-3 (a) - which agrees with our previous results [16]. Pulse widths ranging from about 420 ns to about $1.6 \mu\text{s}$ have been obtained. Fig. 1-3 (b) shows the pulse shape for 100 kHz repetition rate. Note that, at this repetition rate, the pulse is steeper at the falling edge

(about 1.2 μs fall time) compared with the rising edge (2 μs rise time). This characteristic is attributed to the short AOM transmission open time, which limited the pulse width. This explains why the pulse width tends to converge at high repetition rate; in this regime the pulse is cavity dumped. At lower repetition rates, the pulse width also tends to converge. This is due to the fact that, at lower repetition rates, the population inversion accumulation time is long, so before the next AOM transmission comes, the population inversion has already reached its maximum value, which is determined by the Er^{3+} energy level. Considering the pulse width is a function of the population inversion initial and final values [17], the pulse width does not change much as the repetition rate decreases. In the numerical simulation section, we confirm our explanations.

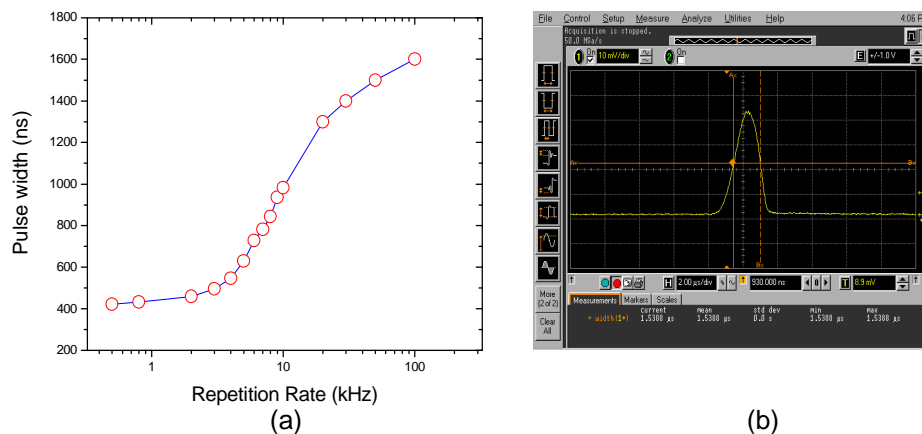


Fig 1-3. (a) Pulse width versus AOM repetition rate and (b) Pulse shape at 100 kHz repetition rate. The pump, signal, and the AOM transmission shape are fixed (including the rise time, on time, and fall time).

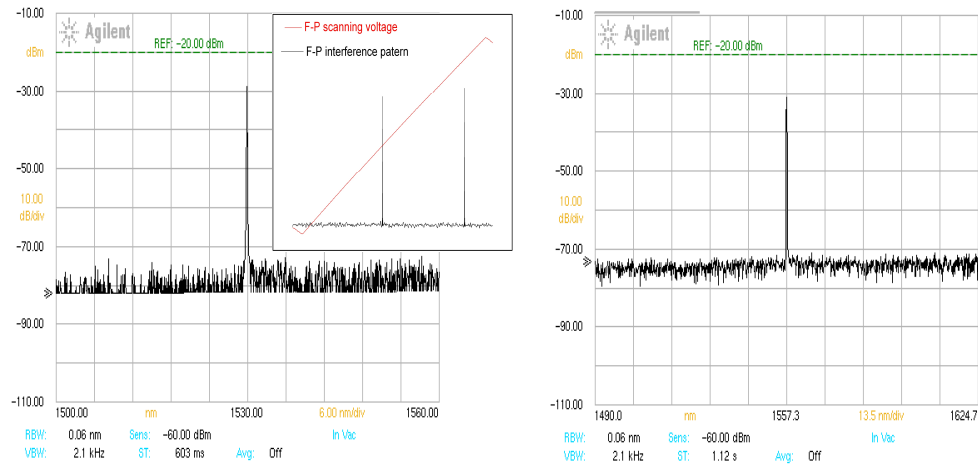


Fig. 1-4. Output pulse spectrum for two different seed injection wavelengths. (a) correspond to 1530 nm seed injection. Insert, Fabry-Parot scanning spectrum; (b) correspond to 1557 nm seed injection.

1.3.3 Transform-limited linewidth

A single-frequency fiber laser at about 1530 nm was used as the injection seed. At 10 kHz repetition rate, the output pulse width is measured to be about 900 ns. The output pulse spectrum was measured by using an optical spectrum analyzer with resolution of 0.06 nm, which is shown in Fig 1-4(a). For different repetition rates, no obvious spectrum changes are observed in the experiment. One can see that the signal-to-noise ratio is about 50 dB. We estimated the linewidth by using a fiber-based Fabry-Perot with a free spectral range (FSR) of 1 GHz and Finesse of ~ 198 [3, 16]. Insert of Fig. 1-4 (a) shows the scanning spectrum for 900 ns Q-switched fiber laser pulses. One can see that the scanning Fabry-Perot

spectrum shows the single burst under transmission peaks of the Fabry-Perot, which corresponds to the line width of < 5 MHz that is the bandwidth limit of the Fabry-Perot interferometer.

In order to demonstrate this injection seeded, Q-switched fiber laser can be operated at other wavelengths in the C-band, a single-frequency fiber laser at 1557 nm and a related bandpass filter were used as an injection seed. The spectrum of the Q-switched pulses with ~ 600 ns duration at 5 kHz is shown in Fig 1-4(b), and the estimated linewidth is transform-limited. It is found that the pulse width tunability at 1557 nm is similar to that at 1530 nm. Therefore, this injection seeded ring cavity Q-switched fiber laser is capable of generating transform-limited pulses in the whole C-band, and the wavelength can be changed or tuned by changing or tuning the single-frequency seed while the output pulses maintain their transform-limited linewidth.

To avoid stimulated Brillouin scattering (SBS), the peak power of the pulses was kept under ~ 10 W by using relatively low pump power. The SBS threshold in this cavity for very narrow spectral output is about 10 W in the ring cavity according to our experiments. For example, using the 30% output coupler shown in Fig 1-1 (a), repetition rates of 0.5 kHz and 100 kHz, produce average/peak powers of 0.12 mW/0.57W and 7.5 mW/0.047W and pulse energies of 0.24 μ J

and $0.075 \mu\text{J}$, respectively.

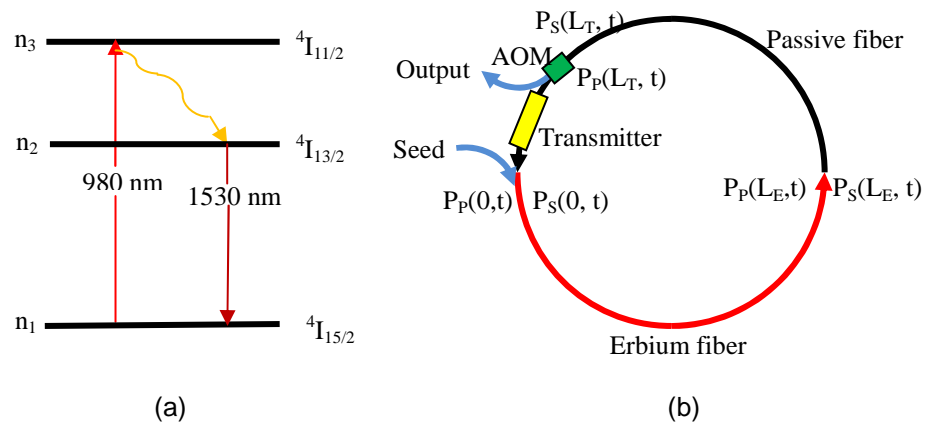


Fig 1-5. (a) Erbium energy level diagram. The pump is at 980 nm, and the laser transition is at 1530 nm. (b) Simplified laser cavity structure for numerical modeling. The beam propagation in the cavity consists of three parts, i.e., propagation in erbium fiber, propagation in the passive fiber, and transmission from all the modules in the cavity.

1. 4 Numerical model

In order to understand the physics of pulse formation and how the pulse characteristics are affected by the cavity parameters and the AOM transmission, we consider the same fiber laser system as described in Section 1.2 but with some simplifications for constructing the numerical simulation model, see Fig 1-5(b). The energy diagram is shown in Fig 1-5(a). We model the pump transition between ${}^4I_{15/2}$ and ${}^4I_{11/2}$, and the laser transition between ${}^4I_{13/2}$ (meta-state) and ${}^4I_{15/2}$. Assuming the transition between ${}^4I_{11/2}$ and ${}^4I_{15/2}$ is very fast, we have $n_3 \approx 0$, where n_3 is the electron population in the ${}^4I_{11/2}$ state. By using a single-frequency fiber laser seed at 1530 nm with a considerable power level, the ASE can thus be ignored. This assumption is valid for this laser cavity, because in the experiments we haven't observed any ASE and the output is still transform-limited at the seed wavelength. In Fig 1-5(b), the simplified cavity model consists of three parts: an Er-doped fiber section, a passive fiber section, and a time-varying transmission section. All the component losses are included in the transmission section, and this simplification is valid since nonlinear effects such as scattering and self-phase modulation are not observed. Then the rate equation for the erbium fiber can be written as [18]:

$$\begin{aligned} \frac{dn_2(z,t)}{dt} = & \frac{P_p(z,t)\Gamma_p}{h\nu_p A} [\sigma_a(\nu_p)n_1(z,t) - \sigma_e(\nu_p)n_2(z,t)] \\ & + \frac{\Gamma_s P_s(z,t)}{h\nu_s A} [\sigma_a(\nu_s)n_1(z,t) - \sigma_e(\nu_s)n_2(z,t)] - \frac{n_2(z,t)}{\tau_{er}}, \end{aligned} \quad (1.1)$$

$$n_{er} = n_1(z,t) + n_2(z,t), \quad (1.2)$$

where, $n_1(z,t)$ and $n_2(z,t)$ are the ground-state and the meta-state population density, n_{er} is the total erbium concentration. $P_p(z,t)$ and $P_s(z,t)$ are the pump power and signal power respectively. Γ_p and Γ_s are the pump and signal overlap factors. ν_p and ν_s are the pump and signal frequencies. $\sigma_a(\nu)$ and $\sigma_e(\nu)$ are the absorption and emission cross sections of the erbium fiber system. A is the doped fiber area, and τ_{er} is the meta-state life time.

Considering only the forward pump and signal at low pump levels and ignoring the nonlinear effects, the pump and signal in the erbium fiber can be described by the traveling-wave model as [14-15]

$$\begin{aligned} \frac{dP_p(z,t)}{dz} + \frac{1}{V_p} \frac{dP_p(z,t)}{dt} = & \Gamma_p [\sigma_e(\nu_p)n_2(z,t) - \sigma_a(\nu_p)n_1(z,t)] P_p(z,t) \\ & - \alpha(\nu_p) P_p(z,t), \end{aligned} \quad (1.3)$$

$$\begin{aligned} \frac{dP_s(z,t)}{dz} + \frac{1}{V_s} \frac{dP_s(z,t)}{dt} = & \Gamma_s [\sigma_e(\nu_s)n_2(z,t) - \sigma_a(\nu_s)n_1(z,t)] P_s(z,t) \\ & - \alpha(\nu_s) P_s(z,t), \end{aligned} \quad (1.4)$$

where V_p and V_s are the group velocity of the pump and signal in the fiber. $\alpha(\nu_p)$ and $\alpha(\nu_s)$ are the pump and signal absorptions. Eqs. (1.1)-(1.4) describe the laser dynamics in the erbium fiber. For the signal and pump dynamics in the passive fiber, it is just

$$\frac{dP_p(z,t)}{dz} + \frac{1}{V_p} \frac{dP_p(z,t)}{dt} = -\alpha(v_p)P_p(z,t), \quad (1.5)$$

$$\frac{dP_s(z,t)}{dz} + \frac{1}{V_s} \frac{dP_s(z,t)}{dt} = -\alpha(v_s)P_s(z,t). \quad (1.6)$$

After the pump and signal propagate through the erbium and passive fibers, a fraction of the signal is coupled out as the output, and the remainder is combined with the injected seed signal as the initial signal power for the next round trip propagation. The boundary conditions for the signal and the pump in the erbium fiber are

$$P_p(0,t) = \eta_p P_p, \quad (1.7a)$$

$$P_s(0,t) = \eta_s P_s + P_s(L_T,t)T(t), \quad (1.7b)$$

where η_p and η_s are the coupling efficiencies for the pump and seed into the erbium fiber. L_T is the total fiber length. $T(t)$ is the total transmission, including the ISOs, band-pass-filter, output coupler, WDM, and the AOM transmission. We can also write the total transmission as

$$T(t) = T_p T_A(t), \quad (1.8)$$

where T_p includes all the components losses including the AOM, couplers, ISOs, WDM, and the band pass filter. $T_A(t)$ is only the time-varying portion of the AOM transmission. As described in Section 2, the transmission can be divided into four parts: rise time (t_r), on time (t_{on}), fall time (t_f) and the off time (t_{off}). In one

period of time, the transmission function can be described by

$$T_A(t) = \begin{cases} 0.5 + 0.5 \sin[\pi(t - 0.5t_r)/t_r], & 0 \leq t \leq t_r \\ 1, & 0 < t - t_r < t_{on} \\ 1 - 0.5 \sin[\pi(t - t_{on} - t_r - 0.5t_f)/t_f], & 0 < t - t_r - t_{on} < t_f \\ 0, & \text{otherwise} \end{cases} \quad (1.9)$$

The passive fiber input signal and pump power is just the output of the signal and pump from the erbium fiber at $z=L_E$. For the signal output, it is extracted after the AOM, so we can write it as

$$P_{out} = P_S(L_T, t)T_A(t). \quad (1.10)$$

Note that, for the actual output there is a fraction in front of the above expression, which is due to the components losses between the output coupler and the Er-doped fiber end; see Fig 1-1(a). The total components loss between the output coupler and the Er-doped fiber end is calculated to be about 5dB. So this fraction is about $10^{-0.5} \approx 0.3$. However, to write the output pulse expression in this way will not affect the numerical simulation results.

Symbol	Value	Symbol	Value
n_{er}	$2.46 \times 10^{25} m^{-3}$	τ_{er}	$10.5 \times 10^{-3} ms$
$\sigma_a(v_P)$	$2 \times 10^{-25} m^2$	λ_P	980 nm
$\sigma_e(v_P)$	0	λ_S	1.53 μm
Γ_P	0.956	P_P	0.8 W
Γ_S	0.838	P_S	10 mW
w_P	$3.2 \times 10^{-2} m$	$\sigma_a(v_S)$	$2.64 \times 10^{-25} m^2$
w_S	$4.2 \times 10^{-2} m$	$\sigma_e(v_S)$	$2.33 \times 10^{-25} m^2$
$\alpha(v_P)$	$0.005 m^{-1}$	A	$5.03 \times 10^{-11} m^2$
$\alpha(v_S)$	$0.005 m^{-1}$	T_P	0.1072

Table 1-1. Summary of the fiber laser parameters.

1.5 Numerical simulation results

In the previous section, the complete theoretical model for simulating the pulse formation is introduced. Eqs. (1.6)-(1.10) govern the pulse formation in the fiber laser cavity, solved using the Runge-Kutta Method [19]. In this part, we first simulate pulse characteristics for different AOM rise times and repetition rates, and compare the results with the experiment. In addition, several other cavity parameters that are not varied in the experiment such as the passive fiber length, and the cavity loss are studied numerically. This study will help us to understand how those parameters change the pulse characteristics, and direct us for future experiments. The parameters used in the simulations are directly from the experiment. The data are summarized in Table 1-1.

1.5.1 Rise time

In this section, we numerically study how the rise time changes the output pulse profile. The pump and the seed power are fixed. The AOM repetition rate is set to 3 kHz and the single pulses for two different AOM rise times are shown in Fig 1-6. As shown in Fig 1-6(a), when the rise time is about 1.5 μ s the pulse exhibits a clear single peak profile. However, when the rise time is only 60 ns, a multi-peak profile is obtained; see Fig 1-6(b). The multi-peak behavior is not as obvious as that observed in the experiment. This might be due to the numerical calculation parameter inaccuracy. But the numerical simulation result is enough to confirm

that the multi-peak behavior that is observed in the experiment is mainly due to the short rise time of the AOM. Thus, the rise time plays an important role in determining the pulse profile. This might also explain the multi-peak pulse observed in Ref [12].

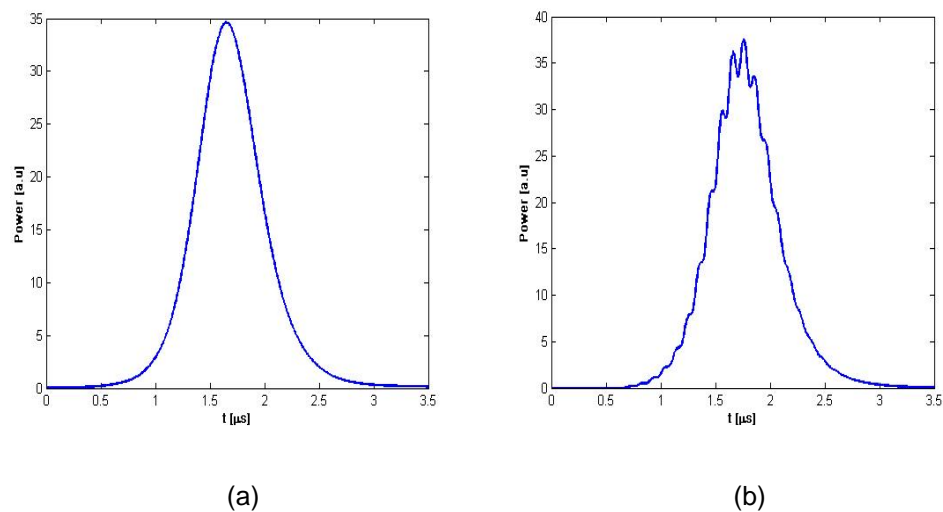


Fig 1-6. Pulse characteristics for different AOM rise time. (a) 1.5 μs rise time; (b) 60 ns rise time.

1.5.2 Repetition rate

This part studies the pulse width for different AOM repetition rates. In Fig 1-7, we plot the calculated FWHM pulse width as a function of the repetition rate. The curve qualitatively follows the experimentally measured results in Fig 1-3(a). The numerically calculated pulse width is about 50% larger compared with the experiment data. There are several reasons for this difference such as the inaccurate estimation of exact pump power and signal power in the erbium fiber,

the erbium fiber absorption and emission cross section data, the actual fiber loss, the ISO extinction ratio, AOM efficiency, actual AOM transmission response, fiber splicing losses, etc. The exact pump power and signal power that are coupled into the cavity are affected by fiber splicing loss, and mode mismatching. The cross section data also varies for different fibers, however, the data we got from the vendor is for different type of Er^{3+} fiber. Previous experiment found that the pump power [16], and inaccurate loss estimation which affect the transmission could result in a large pulse width difference (see the numerical study in Section 1.5.4). From Fig 1-3(a), and Fig 1-7, we note that the pulse width converges for low and high repetition rates and varies in the middle. In order to study this phenomenon, we first plot the output pulse profiles for 4 different repetition rates in Fig 1-8. Figs 1-8(a)-(d) correspond to repetition rates of 3 kHz, 10 kHz, 50 kHz, and 100 kHz, respectively. It can be seen that initially when the repetition is low, the pulse profiles exhibit symmetric characteristics, see Figs 1-8 (a) and (b). However, as the repetition rate increases, the pulse width increases and the profiles exhibit anti-symmetric characteristics. The back side (fall end) of the pulse is limited by the AOM transmission cut-off time See Figs. 1-8 (c) and (d). In the simulation, we used 2 μs on time, and 1.5 μs fall time, which is close to the actual experimental data. This explains the pulse width convergence at high

repetition rate. For low repetition rate, as explained in Section 1.3.2, the population inversion reaches its maximum value at the low Q cavity mode. When the next AOM transmission opens, the pulse width is determined by the initial (maximum) and the final (minimum) population inversion. Thus, at low repetition rate, the pulse width does not change much. In Fig 1-9, the population inversion is plotted for two different repetition rates. At 3 kHz repetition rate (Fig 1-9(a)), the population inversion increases asymptotically, converging to a maximum value. However, at 30 kHz repetition rate the population inversion has not reached the maximum value. So, the numerical simulation results have demonstrated the pulse width vs. repetition rate curve characteristics.

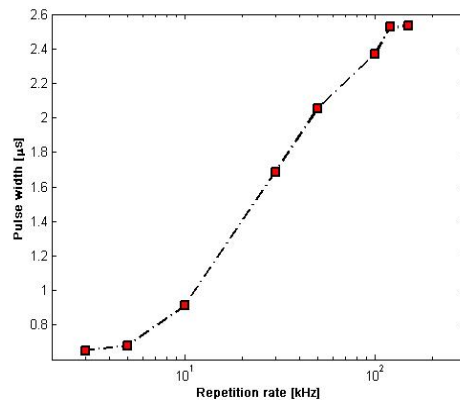


Fig 1-7. Pulse width versus repetition rate.

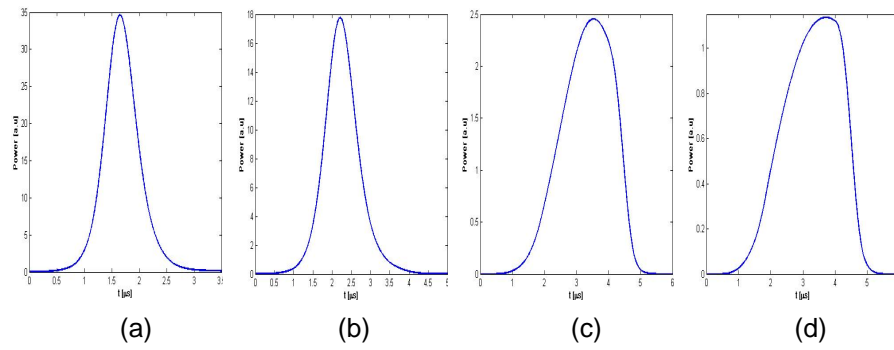


Fig 1-8. Pulse profile at different repetition rate. (a) 3 kHz; (b) 10 kHz; (c) 50 kHz (d) 100 kHz.

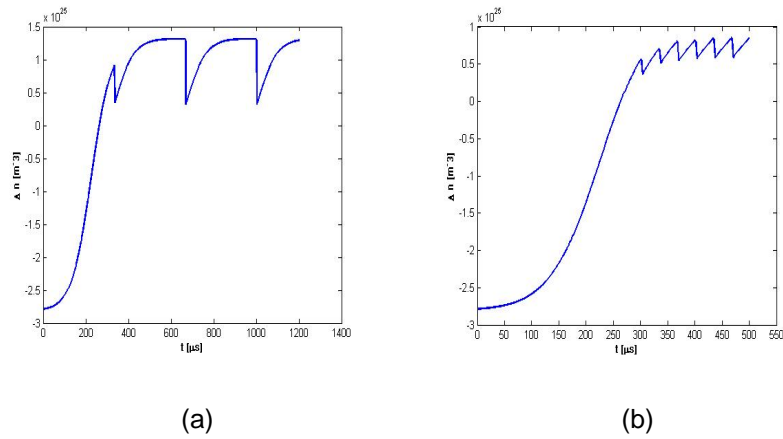


Fig 1-9. Population inversion for two different repetition rates. (a) 3 kHz; (b) 30 kHz.

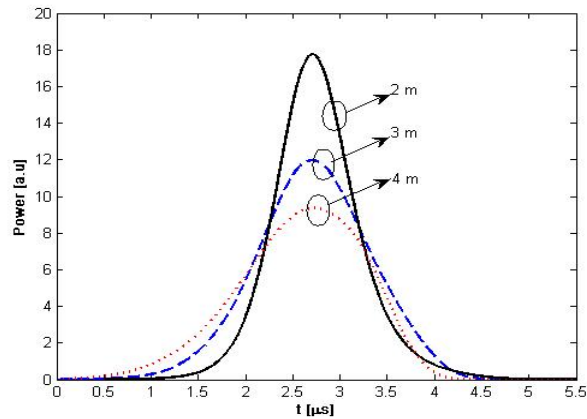


Fig 1-10. Pulse profile for different cavity length. The black line represents 2 meters, the blue dash line represents 3 meter cavity, and the red dash line represents 4 meter cavity.

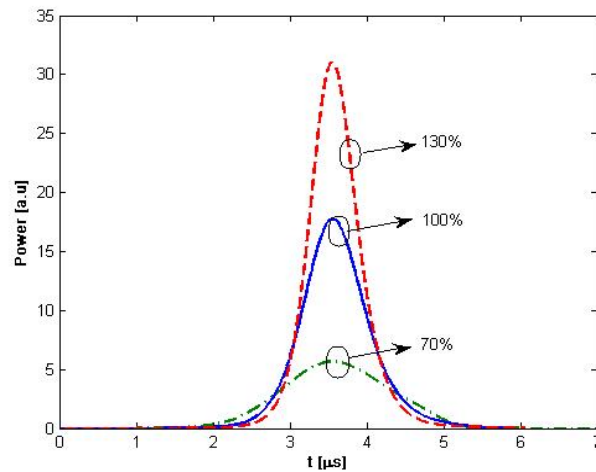


Fig. 1-11. Pulse profile for different cavity loss. The green dash line represents 70 % transmission, the blue line represents original transmission, and the red dash line represents 130% transmission.

1.5.3 Cavity length

In the numerical simulation, the gain fiber length is fixed to be 1 meter. We change the total cavity length by changing the passive fiber length to study how the cavity length changes the pulse profile. In Fig 1-10, the pulse profiles for three different cavity lengths are plotted. The black line, blue dash line, and the red dash line represent 2 meter, 3meter, and 4 meter cavities, respectively. It can be seen that as the cavity length increases, the energy spreads out, increasing the pulse width. The pulse width increase is due to the increase of the cavity photon decay time in the cavity, and this agrees with the Eq (1.17) in Ref [17].

1.5.4 Cavity losses

The cavity loss is mainly determined by the optical component losses, so we

change loss by changing the total component transmission T_P . In Fig 1-11, we plot the pulse profile for 70% T_P (green dash line), 100% T_P (original, blue line), and 130% T_P (red dash line). From this figure, it is found that as loss increases, the pulse energy decreases, and the pulse width increases. However, if the cavity loss is very high, the pulse will not be amplified, so the output pulse would just follow the AOM transmission modulation. So, this explains the pulse width increases at high loss level.

1.6 Conclusion

In conclusion, a SM actively Q-switched, ring cavity, fiber laser has been demonstrated to generate transform-limited pulses based on a single-frequency seed injection ring cavity configuration. This monolithic pulsed fiber laser can be used for spectroscopic sensing and LIDAR systems. The pulse width and wavelength can be tuned simply by controlling the AOM electrical signal trigger and tuning the single-frequency seed injection wavelength, respectively. An AOM was used to actively Q-switch the fiber laser cavity. It has been found that the pulses exhibit multi-peak characteristics when the AOM rise time is short. By tuning the AOM repetition rate, pulse widths ranging from about 400 ns to 1.6 μ s were demonstrated. The wavelength tuning was achieved by changing or tuning the single-frequency fiber laser seed. Numerical simulation results agree well with our experimental results. In addition, the numerical model predicted the pulse characteristics for different cavity losses and lengths.

CHAPTER II

1480 NM RAMAN FIBER LASER

2.1 Introduction

In this section, a cascaded Raman fiber laser is developed for generating output signal at 1480 nm. The Raman laser is achieved by using high reflection grating pairs as the laser cavity mirrors. The Raman gain is provided by a Ge-doped Corning Hi1060 fiber. The laser with output at 1480 nm can be used for optical communication systems for wavelength Multiplexing. Also, this 1480 nm laser can be used as the pump source for Er-doped fiber lasers and amplifiers.

In the experiments, the Yb fiber laser performance is measured. The maximum output power for the Yb fiber laser can reach up to 30 W. With the Raman fiber, and gratings, Raman laser is 1175nm, 1240 nm, 1315 nm, and 1395 nm have been demonstrated. We are currently working towards the last step to achieve lasing at the 1480 nm. Detailed theory and experiment work are presented in the following sections.

2.2 Raman fiber laser theory

When light interact with molecules, it can be inelastically scattered to wavelength different than the incident one. Usually the wavelength is shifted to the longer one. This effect is called Raman scattering which is named after Sir Chandrasekhara Venkata Raman. Raman fiber laser uses Raman scattering which shift the signal frequency to longer wavelength through the so called Stokes Raman scattering.

Raman fiber laser differs from other fiber laser is that it does not use population inversion to achieve laser gain but Raman scattering. The signal amplification and pump dissipation equations are [20, 21]

$$\frac{dP_S(z)}{dz} = g_R P_P(z) P_S(z) - \alpha_S P_S(z), \quad (2.1)$$

$$\frac{dP_P(z)}{dz} = -\frac{\omega_P}{\omega_S} g_R P_P(z) P_S(z) - \alpha_P P_P(z), \quad (2.2)$$

where P_S and P_P are signal and pump power, α_S and α_P are signal and pump absorption coefficients. ω_S ω_P are signal and pump frequencies, respectively. g_R is the Raman gain coefficient which is related to the material properties. For Ge-doped fiber, the Raman gain coefficient peak happens at a frequency shift of 440 cm^{-1} (13.2 THz). However for P-doped fiber, the peak shift is at 1330 cm^{-1} (39.9 THz). Neglecting the pump depletion term in equation (2.2), the signal can be solved as [21]

$$P_S(L) = P_S(0) \exp \left(g_R \frac{P_0}{A_{eff}} L_{eff} - \alpha_S L \right), \quad (2.3)$$

where

$$L_{eff} = \frac{1 - \exp(-\alpha_P L)}{\alpha_P}. \quad (2.4)$$

From Eq (2.3), it can be seen that there is trade-off for between the effective fiber length and the pump loss. In addition, for short fiber length, the effective length approximates L , and for long fiber length, it approximates to $1/\alpha_p$. From this approximation, we can see when use longer fibers, if the pump loss is high, the effective fiber length can be short. So in order to have very large effective length, the pump absorption has to be very low. The best way to get higher gain is to directly increase the Raman gain coefficient.

2.3 Raman fiber laser design

Raman fiber laser using Cascaded cavity design is a good choice for generating wavelength that is not available to the current rare earth fiber laser [22-24]. The Raman fiber laser configuration is depicted in Fig 2-1. Two HR fiber Bragg Grating at 1117 nm constitutes the Yb fiber laser cavity. 11 diode pump lasers are combined to pump the 25-meter Yb fiber. The Raman gain is provided by a 500-meter Corning HI-1060 Raman fiber. The Raman laser has cascaded cavities for 1175 nm, 1240 nm, 1315 nm, 1395 nm, and 1480 nm. The output is achieved by using a partial reflector at 1480 nm.

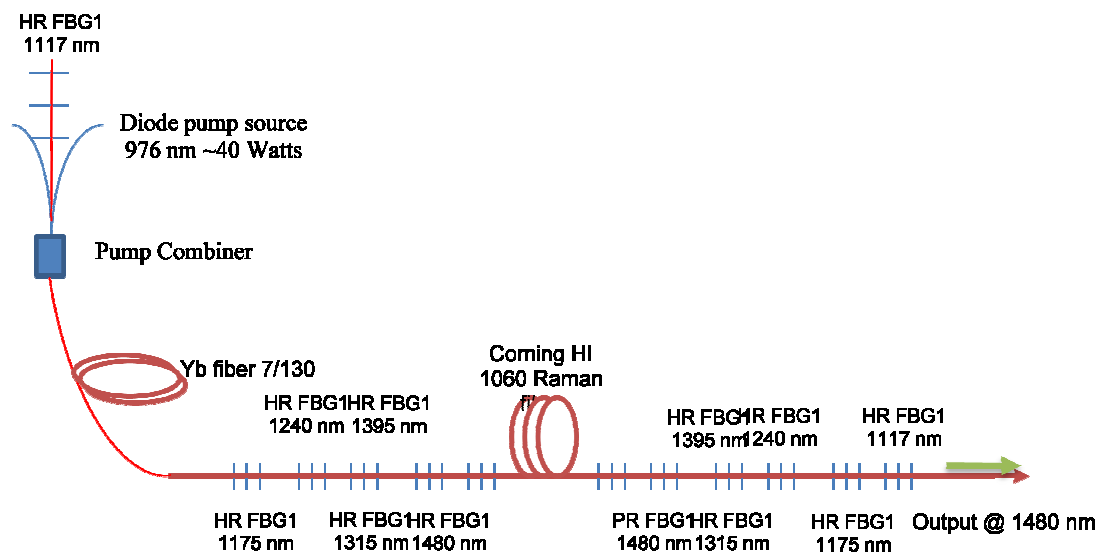


Fig. 2-1. Cascaded Raman fiber laser cavity for generating output signal at 1480 nm.

2.4 Experimental results

In the experiment, we firstly measured the performance of the 975 nm 11-diode combined laser source. The measured output power vs. current is shown in Fig 2-2.

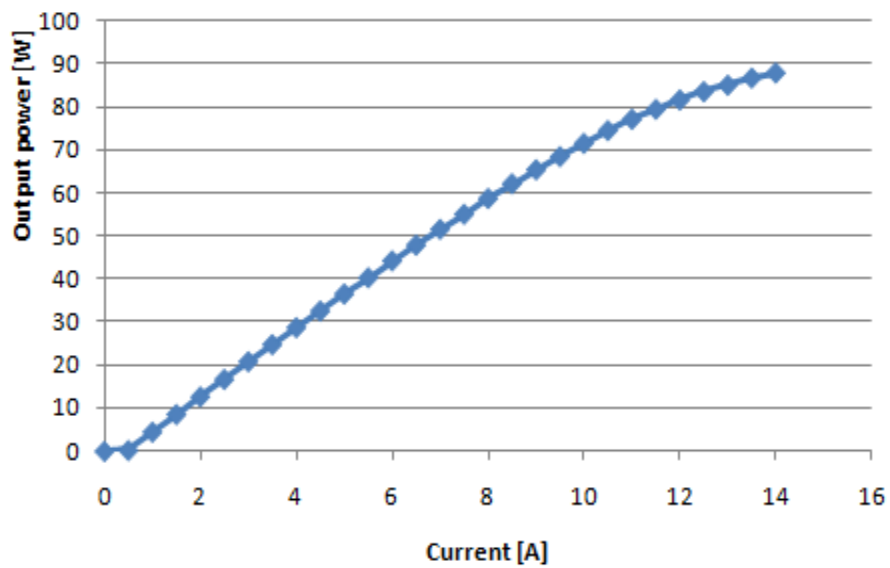


Fig 2-2. The combined 975 nm 11-diode pump laser output.

For the next step, we measured the Yb fiber laser performance. The Yb fiber is pumped with the 975 nm 11-diode pump source. The Yb fiber has HR grating at 1117 nm at one end, and the other end is flat cleaved. The Yb fiber laser slope efficiency curve is shown in Fig 2-3.

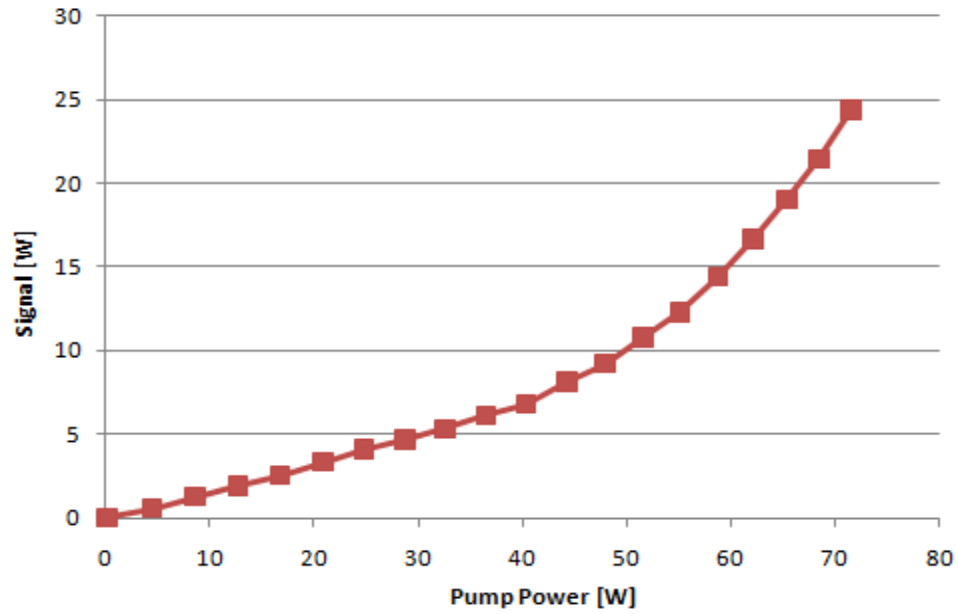


Fig 2-3. The 1117 nm Yb fiber laser output power vs. pump power at 975 nm.

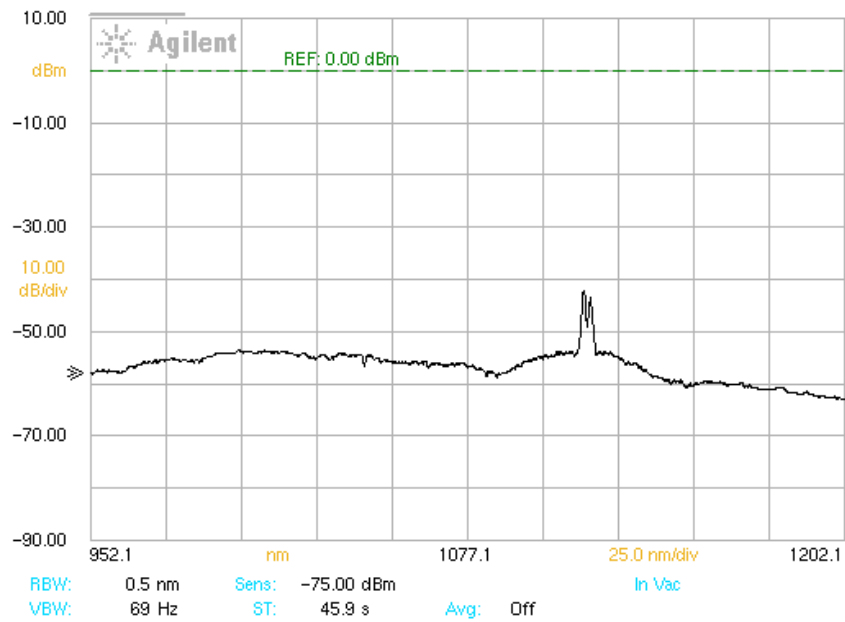


Fig 2-4. The 1117 nm Yb fiber laser spectrum with two HR grating.

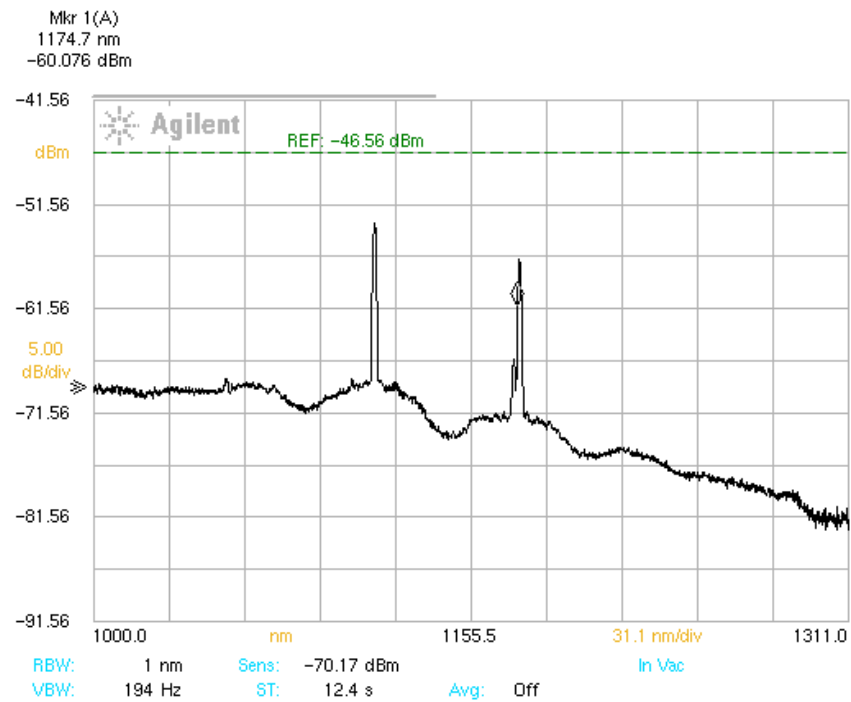


Fig 2-5. The 1175 nm Raman fiber laser.

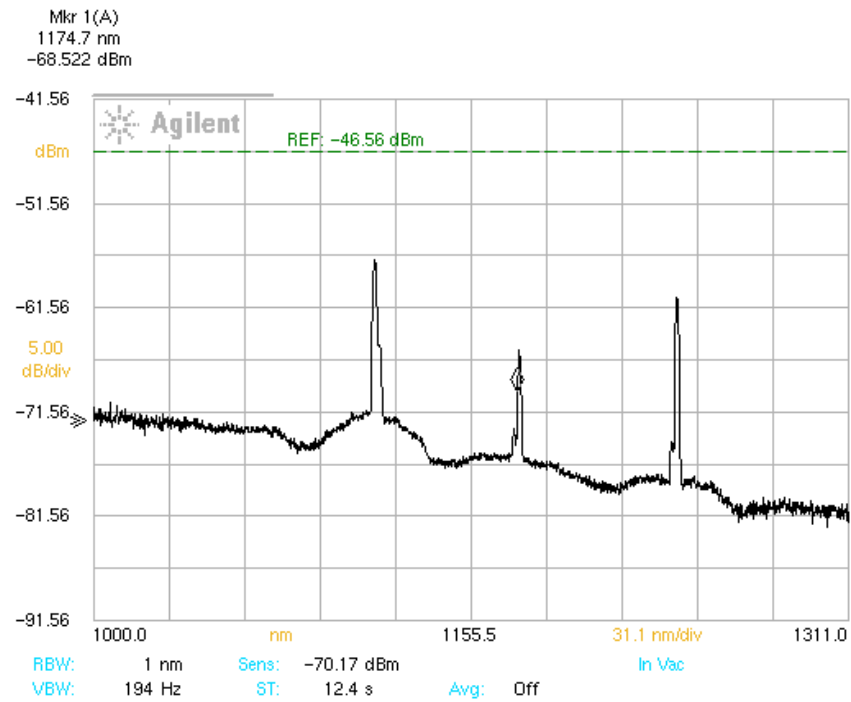


Fig 2-6. The 1175, 1240 nm Raman fiber laser.

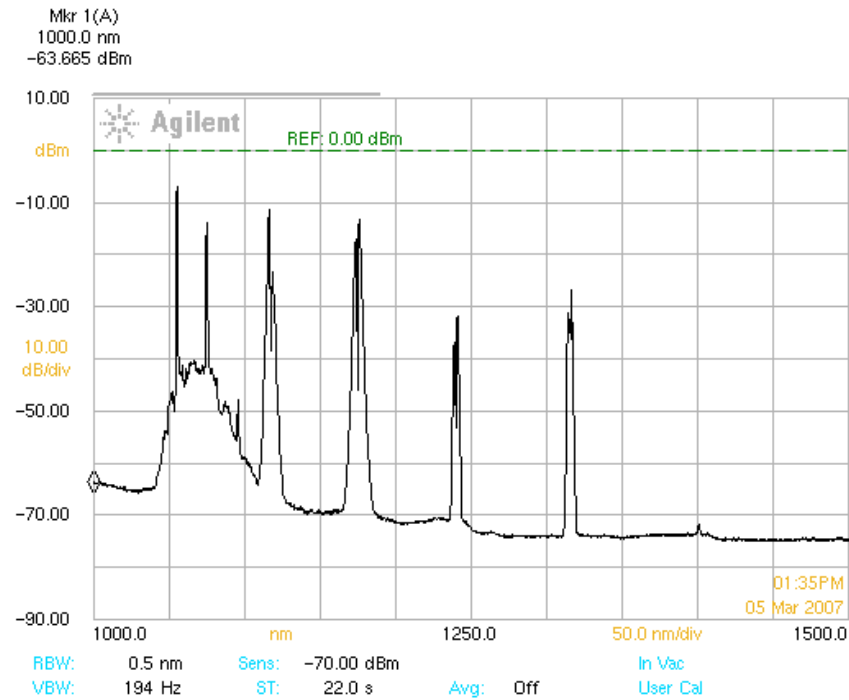


Fig 2-7. The 1175, 1240, 1315 nm Raman fiber laser.

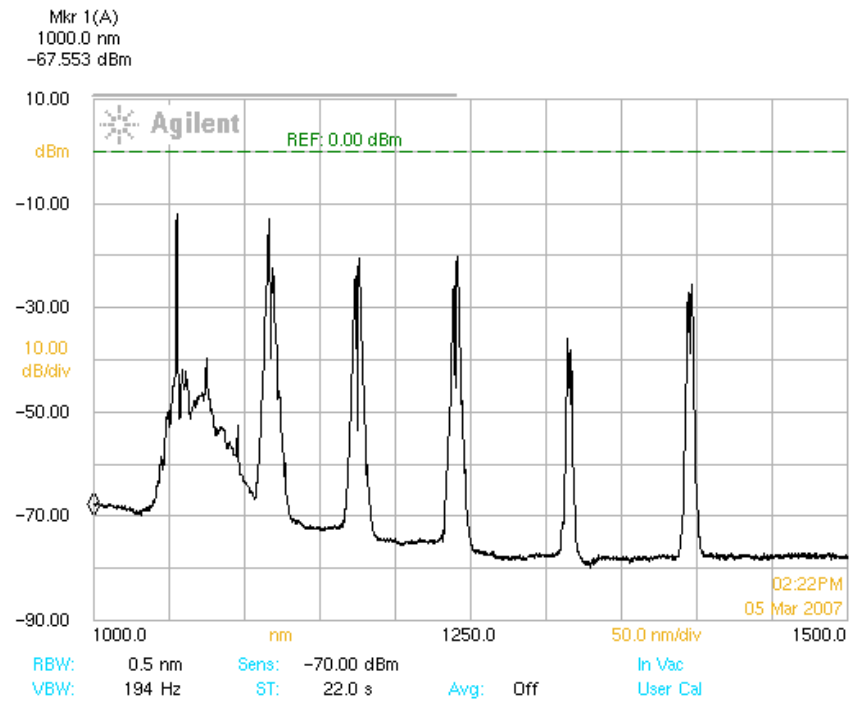


Fig 2-8. The 1175, 1240, 1315, 1395 nm Raman fiber laser.

After testing the Yb fiber laser performance, we started building the Cascaded Raman laser step by step. After splice the second 1117 nm HR grating the cavity output spectrum is shown in Fig 2-4. After adding the 1175 nm grating pair, the Raman laser spectrum shown lasing at 1175 nm in addition to the 1117 nm laser, see Fig 2-5. Figs 2-6, 2-7, 2-8 represent the output spectrum after adding 1240 nm, 1315 nm, and 1395 nm respectively. In order to observe Raman laser at longer wavelength, the 975 nm pump power has to increase. For example, in order to see the 1315 nm Raman laser, the pump power has to be above 45 W, while for 1395 nm Raman laser, the pump is above 60 W. Unfortunately, the Yb fiber and Pump fiber burns at high power. At this point, the 1480 nm grating is not spliced to the cavity yet.

2.5 Conclusion

In this chapter, initial demonstrations on Raman fiber laser have been presented. The current experimental work has demonstrated the generation of output wavelength at 1175 nm, 1240 nm, 1315 nm, and 1395 nm. There are several problems encountered during the experiments. Firstly, at high pump powers the Nufern fiber can be burned at the splice joints, or random places. Secondly, the Raman fiber length needs to be optimized. If the fiber is too long, the signal and pump get absorbed; the output power will be low. If the fiber is too long, the overall Raman gain would be too low not enough to achieve Raman lasing in the cavity. It is suggested to use the OFS Raman fiber because this fiber has higher Raman gain and zero water-peak.

CHAPTER III

FREE SPACE COUPLED FIBER AMPLIFIER

3.1 Introduction

Free space fiber amplifiers and lasers are capable of scaling optical power to Kilo-Watt level [25-27]. In this chapter, a free space fiber amplifier using very short NP highly Er/Yb co-doped phosphate fiber is developed. This fiber amplifier is capable for scaling the signal power while still maintain single-mode, and single frequency output. Using the free space configuration, it allows for better signal and pump coupling to the gain fiber. In particular, a very low numerical aperture and large mode area gain fiber is used as the gain fiber in this experiment, and signal coupling efficiency as high as 90% has been achieved. The signal coupling technique is applied to the supercontinuum generation in a Tellurite fiber.

3.2 Pump and signal free-space coupling into the fiber

There are several factors that limit the signal and pump coupling. The signal coupling is much more difficult due to very small gain fiber core and numerical aperture. There are several factors limit the signal coupling efficiency into the SM fiber. The first one is the mode diameter of the gain fiber. The focus signal beam size has to be smaller than the fiber mode diameter. For single mode fibers, the mode radius can be approximate as [28]

$$w \approx a \left(0.65 + 1.619V^{-\frac{3}{2}} + 2.879V^{-6} \right), \quad (3.1)$$

where a is the core radius of the single mode fiber, the V number is calculated through

$$V = \frac{2\pi a}{\lambda} NA \quad (3.2)$$

where NA is numerical aperture of the fiber, and λ is the signal wavelength in vacuum. For an example, the Er/Yb co-doped phosphate fiber that used for the experiments has a core NA of 0.039 and core radius of 15 μm , the signal wavelength is 1.5586 μm . Apply Eqs 3.1, and 3.2, the V number is calculated to be about 2.36, and the mode diameter is about 33.4 μm .

In order to couple the signal into the gain fiber, a lens can be used to first collimate the signal and use another lens to focus the signal. The focused beam spot size has to be smaller than the fiber mode diameter. However, the smallest

focused beam size cannot be larger than the diffraction limit. The diffraction limited beam size (zero-to-zero) is approximates to be about

$$d = \frac{1.22\lambda}{NA} \quad (3.3)$$

Note that the beam width defined in Eq 3.1 is the 1/e intensity width. However, in Eq 3.3, the beam diameter is defined from the zero-to-zero intensity. From Ref [29], the intensity distribution for airy disk is

$$I = \left(\frac{2J_1(s)}{s}\right)^2 I_0 \quad (3.4)$$

where

$$s = \frac{\pi d NA}{\lambda} \quad (3.5)$$

when $s \approx 3.83$, $I \approx 0$, then the zero-to-zero beam diameter can be obtained as Eq (3.3). It can be also numerically find that when the intensity drops to the 1/e value. $s \approx 1.92$, then the 1/e beam radius can be approximate to be about

$$w = \frac{0.31\lambda}{NA} \quad (3.6)$$

The other factor that limits the signal coupling is the fiber numerical aperture, i.e., NA. In this way, the focus beam NA has to be also smaller than the fiber NA. However, there is trade-off between the NA and the focused beam size. As seen from Eq 3.6, when the NA decreases, the beam radius increases. Thus, in order to obtain maximum signal coupling efficiency, the NA of the beam has to be

optimized.

The pump coupling is much easier since the gain fiber can be cladding pump. However, the pump can burn the gain fiber end at high power. This might be due to the strong absorption at 975 nm pump and the heat generated at the fiber end.

3.3 Experimental results

3.3.1 Experiment set up

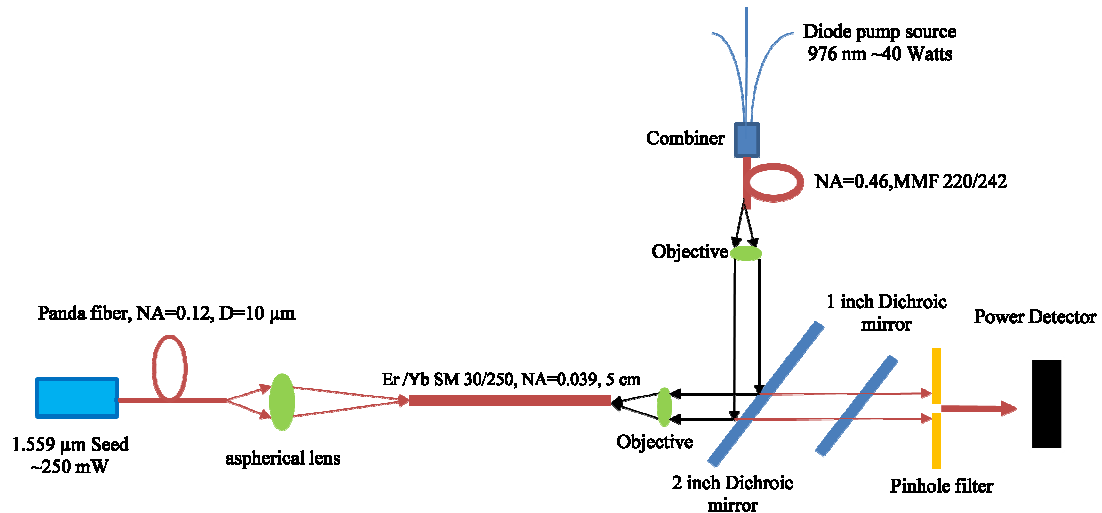


Fig 3-1. The experiment set up for the free space fiber amplifier.

The fiber amplifier set up is described in Fig 3-1. A 975 nm diode pump laser is used to pump the Er/Yb co-doped phosphate fiber from the right end. The pump laser is delivered by a MM fiber with NA=0.46, core size of 220 μm . Two objective lenses are used to couple the pump into the gain fiber. Note that the objective lenses used are not AR-coated at 975 nm. The measured pump power loss for each one is about 30%, so the total pump power loss is up to 50%. The signal is delivered by a panda fiber with NA=0.12, and core size of 10 μm . In this fiber, the V number is about 2.41, and the mode radius is about 5.47 μm . The seed is coupled to the gain fiber through an aspheric lens at imaging condition. The image condition is optimized such that the seed's numerical aperture in image

space is close to the NA of the Er/Yb fiber, as well as the focused size is smaller than the gain fiber mode size. It is found that when the image distance to object distance ratio is about 3, the coupling is optimized. At this point, using Eq. 3.6, the focused beam size is about $24\ \mu\text{m}$, and the NA is about 0.04. The Er/Yb fiber is flat cleaved at both ends and a pinhole filter is used to filter the cladding mode from the Er/Yb fiber. Most importantly, this filter is very useful for optimized the seed coupling.

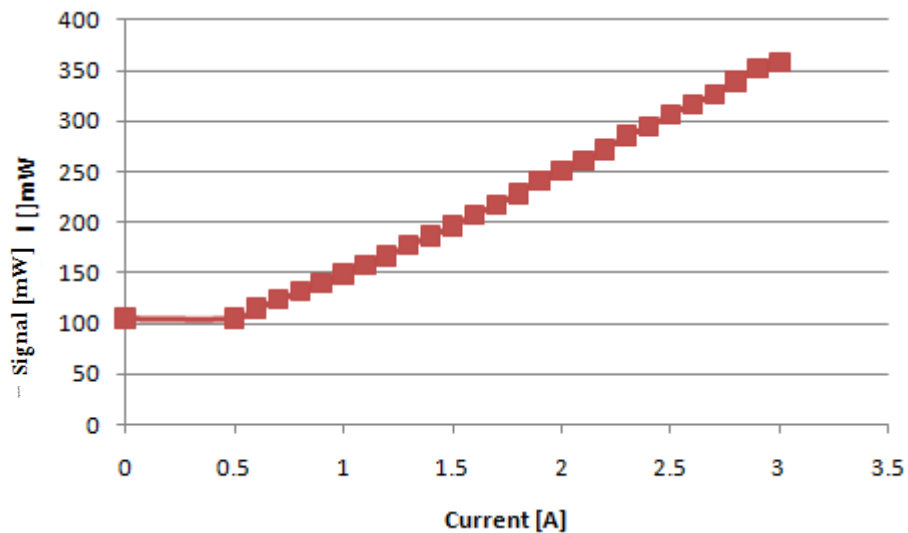


Fig 3-2. Output signal power vs. pump current.

3.3.2 Amplified signal

For a 5 cm section of Er/Yb fiber and 220 mW seed power, we measured the signal vs. pump current curve; see Fig 3-2 (assuming 30% absorption of the signal by the objective lens). It can be seen that as the pump current increases,

the output signal as increases linearly. There has been no pump saturation observed. The pump power at 3.5 A is about 10 W, however the gain fiber end burns at power higher than 10 W.

3.3.3 Signal coupling and absorption

In this sub-section, the technique to optimize the signal coupling efficiency is introduced. Measurement on signal absorption coefficient is done in order to estimate the signal coupling efficiency into the fiber core.

There are several steps for optimized the signal coupling efficiency. For a specific seed image condition, the first step is to use a power detector to optimize the signal coupling. Adjusting the translation stages for the seed fiber, aspheric lens until observe a maximum optical power at the detector. However, at this point, the seed may have been mostly coupled into the gain fiber cladding. The next step is turn on the pump (assuming the pump coupling has been optimized), use a pinhole detector as indicated in Fig 3-1. The pinhole detector only passes a small radius of signal from the center, thus blocking the cladding mode. Then, finely adjusting the signal coupling translation stages, until the power at the detector reaches maximum. When the signal is coupled into the gain fiber core, the power is very sensitive to the signal alignment.

After all this work, what we called the local optimization is finished. In order to optimize the signal coupling efficiency globally, we need to optimize the seed

image condition. Through adjusting the seed image condition, the signal numerical aperture and focus spot size and be adjusted for improving the coupling to the gain fiber. Usually, in order to change the image condition, We first move the aspheric lens position along the optical axis, and then adjust the seed fiber until the detected power reaches maximum which indicates the signal is coupled into the gain fiber.

There is no direct way of estimate the seed coupling efficiency, so in order to estimate the coupling efficiency, the signal absorption in the gain fiber has been made. The absorption coefficient is measured through Bill's Law. We keep the same input signal power for two same fibers but different length. Let the input power for both fibers be P_0 , the measured output power for fiber 1 is P_1 , for fiber 2 is P_2 . If the lengths for the fibers are L_1 and L_2 , then from Bill's Law $P_1 = P_0 e^{-\alpha L_1}$, and $P_2 = P_0 e^{-\alpha L_2}$. By simplification, we have $\frac{P_1}{P_2} = e^{-\alpha(L_1-L_2)}$, then finally, we reached

$$\alpha = \ln \left(\frac{P_2}{P_1} \right) / (L_1 - L_2) \quad (3.7)$$

When the unit for length is cm, then the absorption coefficient is cm^{-1} . For optical fibers, the absorption is usually measured in dB/cm. The conversion between both units is

$$\alpha(\text{dB/cm}) \approx 4.343 \alpha (1/\text{cm}) \quad (3.8)$$

During the experiment, three independent measurements for absorption are

Trial	Fiber 1 length (cm)	Fiber 2 length (cm)	P1 (mW)	P2 (mW)	Absorption (1/cm)
1	3.7	5.5	33	14	0.48
2	5.2	7.4	24	10	0.4
3	5.2	8	24	7	0.44

Table 3-1. Signal absorption measurement in the Er/Yb fiber.

done, and the data are summarized in Table 3-1. From this table, the average absorption can be calculated to be 0.44 (1/cm), i.e., 1.91 dB/cm. From Bill's Law, the coupled power into the fiber can also be calculated. This coupled power can be used to determine the coupling efficiency. The signal before entering the gain fiber is measured to be 260 mW. From Table 3-2, it can be concluded that signal coupling efficiency can reach up to 91% in the Er/Yb fiber. One may ask why the coupling efficiencies are different for different trials. The reason is because, for each trial the system alignment has changed. So it is not possible to get the best signal coupling efficiency every time, and it takes time to achieve the best signal coupling.

Trial	Coupled power (mW)	Coupling efficiency (%)
1	195	75
2	192	74
3	237	91

Table 3-2. Signal coupling efficiency to the Er/Yb fiber.

3.4 Nonlinearity study in Thulium fiber using free space coupling technique

Previous experimental results demonstrated the ability of achieving very high coupling efficiency using free space signal coupling. Tellurite fiber is a good candidate for supercontinuum generation [30]. In this part, using free space coupling techniques, some initial results for supercontinuum generation in Tellurite fibers are presented.

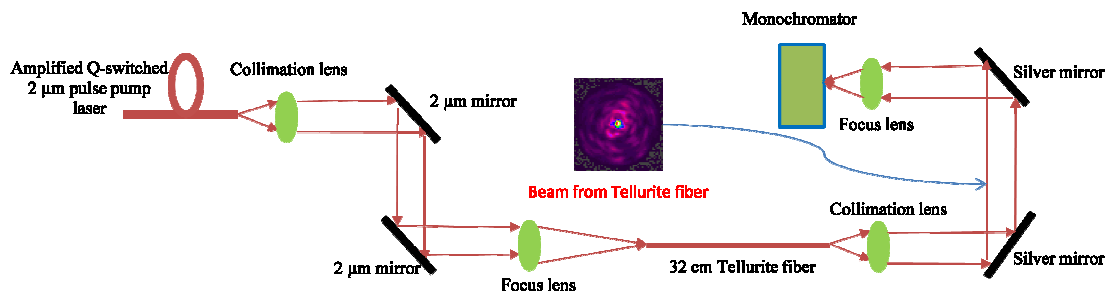


Fig 3-3. Experiment set up for supercontinuum generation in Tellurite fiber.

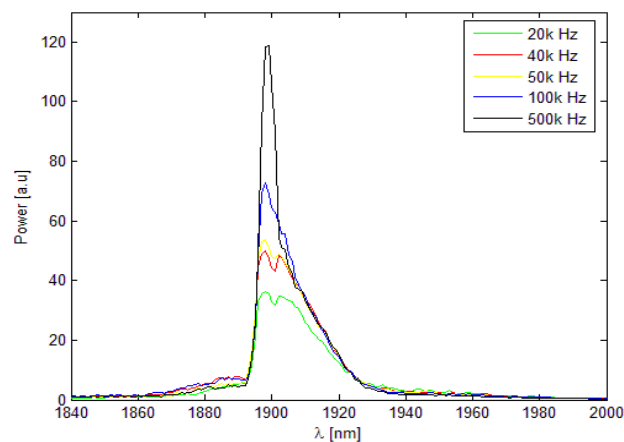


Fig 3-4. The output spectrum at different pump laser repetition rates.

The experiment set up for the free-space supercontinuum generation in

Tellurite is presented in Fig 3-3. A MOPA-based Q-switched 2 μm laser is used as the pump to the tellurite fiber. The output spectrum from the Tellurite fiber is measured with a monochromator. The insert shows the measured beam profile from the out of the Tellurite fiber using a Spiricon Camera.

3.5 Conclusion

In this chapter, the issues on the development of free space fiber amplifier are discussed. The two factors, i.e., beam focus size and numerical aperture, which affect the signal coupling efficiency to the gain fiber, are studied. Experimental techniques for achieving high signal coupling efficiency are presented. Experimental results achieved signal coupling efficiency into the gain fiber to be as high as 90%. The technique in signal coupling is applied to the supercontinuum generation in Tellurite fibers. Fiber nonlinearities that broadened the signal spectrum is observed, which indicates excellent signal coupling into the Tellurite fiber. The future work is to prevent the fiber burning at high pump power. There two several ways to achieve this. For example, the gain fiber can be pump at both fiber ends, then twice of the maximum pump power can be coupled to the gain fiber. In order to avoid high absorption at 975 nm pump, 1480 nm pump laser source can be developed.

CHAPTER IV

CONCLUSION AND FUTURE WORK

In this thesis, a Q-switched ring cavity fiber laser is developed to achieve transform-limited laser output. The output pulse width is tunable over a long range, and the signal frequency can be tuned in the whole C band as well. In addition, we have developed a numerical model to successfully repeat the experimental results. The numerical model also provides a way for us to study how the cavity parameters can change the laser output pulse characteristics. In the future, experimental work can be done for studying how the pulse characteristics are affected by the cavity loss, and length. The experimental results can be compared with the numerical simulation results presented in this thesis.

Following the Q-switched laser, a Raman fiber laser is introduced. This Raman fiber laser is used to generate signal at the 1480 nm. Principle on how the Raman fiber laser works is briefly introduced. The experimental results have achieved Raman fiber laser at 1175 nm, 1240 nm, 1315 nm, and 1395 nm. In the future, the Raman fiber length can be optimized to achieve Raman lasing at lower pump threshold. The Raman fiber laser system can also be slightly modified for better performance. For example, a partial reflection grating at 1117

nm can be used to build the Yb fiber laser, and then the 1117 nm Yb fiber laser can be separated from the Raman fiber laser cavities, avoiding setting the Raman fiber laser cavities in the 1117 nm Yb fiber laser cavity. This will improve the Yb fiber laser efficiency.

In chapter 3, we studied a free space fiber amplifier system using the Er/Yb doped phosphate NP fiber. The technique for achieving high signal coupling efficiency is discussed in detail. In the experiment, we have demonstrated signal coupling efficiency can be up to 90% in the fiber. This signal coupling technique to used to study super-continuum generation in a tellurite fiber. Currently, the issue that limits the signal power scaling in the gain fiber is the gain fiber burning which has limited the pump power that can be launched into the gain fiber. The future work is to prevent the fiber burning at high pump power. In order to avoid fiber burning at 975 nm pump, 1480 nm pump laser source can be developed. At 1480 nm pump, the pump absorption will be lower which may relieve the gain fiber end. Another way to increase the pump power to the gain fiber is to pump the gain fiber at both ends of the gain fiber.

REFERENCES

1. N. P. Barnes, B. M. Walsh, D. J. Reichle, and R. J. DeYoung, "Tm: fiber laser for remote sensing," *Opt. Mater.* **31**, 1061 (2009).
2. R. J. De Young, and N. P. Barnes, "Profiling atmospheric water vapor using a fiber laser lidar system," *Appl. Opt.* **49**, 562-567 (2010).
3. W. Shi, E. B. Petersen, D. T. Nguyen, Z. Yao, J. Zong, M. A. Stephen, A. Chavez-Pirson and N. Peyghambarian, "Kilowatt-level SBS-threshold monolithic transform-limited 100 ns pulsed fiber laser at 1530 nm," *Opt. Lett.* **35**, 2418-2420 (2010).
4. D. A. Kliner, J. P. Koplrow, R. L. Farrow, P. E. Schrader, S. W. Moore, T. A. Reichardt, A. A. Hoops, T. J. Kulp, K. M. Armstrong, R. L. Sommers, P. Schultz, L. Goldberg, and J. Fève, "Fiber-Based Laser Systems for Spectroscopic Trace-Gas Detection," in *Laser Applications to Chemical, Security and Environmental Analysis*, OSA Technical Digest (CD) (Optical Society of America, 2008), paper LTuA3.
5. E. B. Petersen, W. Shi, D. T. Nguyen, Z. Yao, J. Zong, A. Chavez-Pirson, and N. Peyghambarian, "Enhanced terahertz source based on external cavity difference-frequency generation using monolithic single-frequency pulsed fiber lasers," *Opt. Lett.* **35**, 2170-2172 (2010).
6. E. B. Petersen, W. Shi, A. Chavez-Pirson, N. Peyghambarian, and A. T. Cooney, "Efficient parametric terahertz generation in quasi-phase-matched GaP through cavity enhanced difference-frequency generation," *Appl. Phys. Lett.* **98**, 121119 (2011).
7. Mario Auerbach, Peter Adel, D. Wandt, Carsten Fallnich, S. Unger, S. Jetschke, and H. Mueller, "10 W widely tunable narrow linewidth double-clad fiber ring laser," *Opt. Express* **10**, 139-144 (2002).
8. Y.-X. Fan, F.-Y. Lu, S.-L. Hu, K.-C. Lu, H.-J. Wang, G.-Y. Zhang, and X.-Y. Dong, "Narrow-linewidth widely tunable hybrid Q-switched double-clad fiber laser," *Opt. Lett.* **28**, 537-539 (2003).

9. C. Cuadrado-Laborde, P. Pérez-Millán, M. V. Andrés, A. Díez, J. L. Cruz, and Yu. O. Barmenkov, "Transform-limited pulses generated by an actively Q-switched distributed fiber laser," *Opt. Lett.* **33**, 2590-2592 (2008).
10. R. J. Williams, N. Jovanovic, G. D. Marshall, and M. J. Withford, "All-optical, actively Q-switched fiber laser," *Opt. Express* **18**, 7714-7723 (2010).
11. D. Popa, Z. Sun, T. Hasan, F. Torrisi, F. Wang, and A. C. Ferrari, "Graphene Q-switched, tunable fiber laser," *Appl. Phys. Lett.* **98**, 121119 (2011).
12. P. D. Dragic, "Injection-seeded Q-switched fiber ring laser," *IEEE Photon. Technol. Lett.* **16**, 1822-1824 (2004).
13. P. D. Dragic, "Wavelength switching dynamics in injected fiber ring lasers," *J. Appl. Phys.* **101**, 033101 (2007).
14. S. Adachi, and Y. Koyamada, "Analysis and design of Q-switched Erbium-doped fiber laser and their application to OTDR," *IEEE Photon. Technol. Lett.* **20**, 1506-1511 (2002).
15. Y. Wang and C. Q. Xu, "Actively Q-switched fiber lasers: switching dynamics and nonlinear processes," *Prog. Quantum Electron.* **31**, 131 (2007).
16. W. Shi, E. B. Petersen, M. Leigh, J. Zong, Z. Yao, A. Chavez-Pirson, and N. Peyghambarian, "High SBS-threshold single-mode single-frequency monolithic pulsed fiber laser in the C-band," *Opt. Express* **17**, 8237-8245 (2009).
17. J. J. Degnan, "Theory of the optimally coupled Q-switched laser," *IEEE J. Quantum Electron.* **25**, 214-220 (1989).
18. C. R. Giles and E. Desurvire, "Modeling erbium-doped fiber amplifiers," *J. Lightwave Technol.* **9**(2), 271-283 (1991).
19. J. D. Lambert, *Numerical methods for ordinary differential systems: the initial value problem* (John Wiley & Sons, Inc. New York, NY, 1991).

20. Y. Kang, "Calculations and Measurements of Raman Gain Coefficients of Different Fiber Types," M.S. thesis, Dept. Electrical Engineering, Virginia Polytechnic Inst., Blacksburg, VA.
21. R. H. Stolen, "Fiber Raman lasers", *Fiber and Integrated Optics*, **3**: 1, 21 — 51(1980)
22. J. W. Nicholson, M. F. Yan, P. Wisk, J. Fleming, F. DiMarcello, E. Monberg, T. Taunay, C. Headley, and D. J. DiGiovanni, "Raman fiber laser with 81 W output power at 1480 nm," *Opt. Lett.* **35**, 3069-3071 (2010)
23. N. S Kim, M Prabhu, C. Li, J. Song, and K. Ueda, " 1239/1484 nm cascaded Phosphosilicate Raman fiber laser with CW output power of 1.36 W at 1484 nm pumped by CW Yb-doped double-clad fiber laser at 1064 nm and spectral continuum generation," *Opt. Commun.* **176**, 219 (2000).
24. Y. Feng, L. R. Taylor, and D. B. Calia, "150 W highly-efficient Raman fiber laser," *Opt. Express* **17**, 23678-23683 (2009).
25. G. D. Goodno, L. D. Book, and J. E. Rothenberg, "Low-phase-noise, single-frequency, single-mode 608 W thulium fiber amplifier," *Opt. Lett.* **34**, 1204-1206 (2009).
26. Y. Jeong, J. K. Sahu, D. B. S. Soh, C. A. Codemard, and J. Nilsson, "High-power tunable single-frequency single-mode erbium:ytterbium codoped large-core fiber master-oscillator power amplifier source," *Opt. Lett.* **30**, 2997-2999 (2005).
27. Y. Jeong, J. Sahu, D. Payne, and J. Nilsson, "Ytterbium-doped large-core fiber laser with 1.36 kW continuous-wave output power," *Opt. Express* **12**, 6088-6092 (2004).
28. G. P. Agrawal, *Fiber-Optic Communication Systems*, John Wiley & Sons, Inc., New York, (2002).
29. C. D Meinhart, and S. T. Wereley, "The theory of diffraction-limited resolution in microparticle image velocimetry," *Meas. Sci. Technol.* **14** 1047-1053 (2003).

30. P. Domachuk, N. A. Wolchover, M. Cronin-Golomb, A. Wang, A. K. George, C. M. B. Cordeiro, J. C. Knight, and F. G. Omenetto, "Over 4000 nm bandwidth of mid-IR supercontinuum generation in sub-centimeter segments of highly nonlinear tellurite PCFs," *Opt. Express* **16**, 7161-7168 (2008).